Reactivity of the monocyte/macrophage system to superparamagnetic anionic nanoparticles

Nathalie Luciani, Florence Gazeau, Claire Wilhelm

Reactivity of the monocyte/macrophage system to superparamagnetic anionic nanoparticles†

Nathalie Luciani, Florence Gazeau and Claire Wilhelm*

Received 17th February 2009, Accepted 17th April 2009
First published as an Advance Article on the web 8th June 2009
DOI: 10.1039/b903306h

Nano-scale magnetic materials are increasingly being used in the biomedical field for medical imaging, drug-delivery, magnetic sorting, and therapeutic hyperthermia. In particular, magnetic cell labelling offer attractive possibilities for MRI cell imaging, allowing the tracking of a cell population in living animals. Understanding of the interaction of nanoparticles with cells is then of paramount importance. Here, we characterize the uptake of anionic magnetic nanoparticles by THP1 monocytes and derived macrophages. The incorporation of nanoparticles was assessed by electron microscopy. Cell capture was then quantitated as a function of incubation time and extracellular iron. A simple binding–internalisation mechanism allowed modelling all uptake curves, leading to the affinity constants, the maximal mass that can adsorb on the cell membrane, the internalisation time constants and capacities. Though the adsorption step was comparable for monocytes and macrophages, the latter exhibited a more than ten times higher endocytotic activity. For both cell types, we report an excellent efficiency of the magnetic label, with a maximum load of 6 pg_{Fe} $cell^{-1}$ in monocytes and almost 50 pg_{Fe} $cell^{-1}$ in derived macrophages. Finally, we demonstrated that endocytosed nanoparticles did not affect differentiation of labelled monocytes into macrophages.

Introduction

Based on unique physical, chemical, thermal and mechanical properties, magnetic nanoparticles are among the first nanoscale materials to be used in the field of biomedicine. Indeed, these multifunctional agents have opened a realm of applications ranging from cell sensing, biodetection or cell separation, to drug delivery, tissue engineering, MRI contrast enhancement and magnetically induced thermotherapy. In particular, the fact that nanoparticles exhibit the same sizes as proteins (typically 5 nm), much inferior to the ones of a living cell (approximately 10 μm), makes them extremely suitable for cell "tagging". This last decade, labelling with magnetic nanoparticles has become a method of choice for *in vivo* MRI tracking of cell transplant or migration.[1] Among the most popular approaches for MRI cell imaging, important issues concern the visualisation of stem cell homing to target organs, fundamental for evaluating stem cell-based therapies[2] and the assessment of immune cell recruitment in infected areas.[3–5] The monocyte–macrophage system consists of macrophages and their precursor cells, monocytes, all derived from hematopoietic stem cells. After differentiation, monocytes enter the circulation and migrate into various tissues where they differentiate into macrophages. Macrophages then play a central role in various inflammatory diseases, including sclerosis, ischemic stroke lesions, transplanted graft rejection, bacterial infections, and others. There is therefore a real clinical need for imaging the depiction of monocytes and macrophages during the immune reaction *in vivo*. Monocytes recruitment into infection sites or within hypoxic regions of tumors may also be exploited for nanoparticles based delivery: monocytes could serve as Trojan horses for transporting therapeutic nanoparticles.[6,7]

Understanding of particles interactions with immune cells on the nanoscale level then appears as a strong requisite behind the development of imaging and therapeutic applications. This last decade, we investigated the use of a new class of magnetic nanoparticles (anionic citrate-coated maghemite nanoparticles) as contrast agents for MRI cell imaging.[8] We have shown that these negatively charged magnetic nanoparticles are extremely efficient for labeling most cell types *in vitro*, including primary and secondary cultured cells, therapeutic cells, malignant cells, muscle cells. They are challenging the use of nanoparticles covered with a layer of polymers, which often require the addition of a transfecting agent to enter the cells. The high efficiency of anionic nanoparticles cell uptake was found to be due to their strong and non-specific adsorption to the plasma membrane which precedes the internalisation step. Here we propose a comprehensive description for cell uptake of anionic maghemite nanoparticles as a function of the differentiation state of human monocytes. We use the *in vitro* THP1 human cell model system, which accurately mimics human blood monocytes. After treatment with phorbol esters, THP1 monocytes differentiate into macrophage-like cells which resemble native human macrophages with regard to extensive criteria such as morphological characteristics or expression of membrane antigens and receptors. Uptakes of nanoparticles by monocytes and macrophages were quantitated, compared and described with a single two-step model for both cell types. Moreover, the morphology and gene expression of macrophages derived from magnetically

Laboratoire Matière et Systèmes Complexes (MSC), UMR 7057 CNRS, University Paris Diderot, Paris, France. E-mail: claire.wilhelm@univ-paris-diderot.fr

† This paper is part of a *Journal of Materials Chemistry* theme issue on inorganic nanoparticles for biological sensing, imaging, and therapeutics. Guest editor: Jinwoo Cheon.

labelled monocytes were monitored to assess the influence of the magnetic nanoparticles label on the differentiation process.

Materials and methods

Anionic maghemite nanoparticles

Nanoparticles were synthesised according to the Massart procedure by alkaline coprecipitation of iron chloride salts. The so obtained ionic precursor composed of magnetite (Fe_3O_4) nanoparticles was then oxidised into maghemite (γ–Fe_2O_3) nanoparticles. As a second step, for biomedical applications, nanoparticles are chelated with citrate which confers to the nanoparticles negative surface charges (COO–) at pH 7 (zeta potential −30 mV), ensuring colloidal stability in biological media through electrostatic repulsion. The nanoparticles have a mean diameter of 7.5 nm with a polydispersity index of 0.35 and are composed of about 13 250 iron atoms. Their hydrodynamic size, determined by dynamic light scattering, is about 30 nm. The amount of nanoparticles in a biological sample can be expressed in pg of iron, 1 pg then corresponding to 0.8 millions of nanoparticles. Each nanoparticle exhibits superparamagnetic behaviour and carries an effective magnetic moment at saturation that can be calculated as the product of the saturation magnetisation of maghemite ($Ms = 3.1 \times 10^5$ A m^{-1}) and the volume of the nanoparticle.

Cell culture, cell differentiation and magnetic labelling

The human myelomonocytic THP1 cell line was cultured in suspension (from 0.2 to 1 million cells ml^{-1}) in RPMI 1640 medium containing 10% (v/v) fetal bovine serum supplemented with 2 mM L-glutamine and 100 U ml^{-1} penicillin–streptomycin at 37 °C in 5% CO_2. Cells were used between passages 25 and 35. Under treatment with phorbol ester (PMA 50 ng ml^{-1}, 4 millions cells in 5 ml), THP1 cells adhere to cell culture flasks and differentiate into macrophages. Cells were stimulated with PMA for 6 days to become fully differentiated macrophages before use in experiments.

For magnetic labelling, anionic maghemite nanoparticles were dispersed in serum free RPMI supplemented with 5 mM citrate sodium at iron concentrations ranging from 0.5 to 10 mM and incubated with THP1 monocytes and derived macrophages for 15 min to 4 h. Incubation was performed either at 4 °C to inhibit the internalisation process and explore solely the nanoparticle interactions with cell membranes, or at 37 °C to analyse the whole cell capture. After labelling, monocytes in suspension were collected by centrifugation and washed two additional times while adherent macrophages were washed twice, detached with trypsin and resuspended in complete medium.

To assess the localization of the magnetic nanoparticles within the cells, transmission electron microscopy (TEM) was performed on pellets of 1 million cells, fixed with 2% glutaraldehyde in 0.1 M sodium cacodylate buffer, postfixed with 1% osmium tetroxide containing 1.5% potassium cyanoferrate, gradually dehydrated in ethanol, and embedded in Epon. Ultrathin sections of 70 nm are examined with a Zeizz EM902 microscope (INRA, Plateform MIMA2, Laboratoire de Génomique et Physiologie de la Lactation, Jouy en Josas, France).

Quantification of the cell magnetic load: Single cell magnetophoresis

When submitted to a magnetic field gradient gradB, a magnetically labelled cell of magnetic moment M_{cell} is driven into movement towards the stronger field, under the effect of the magnetophoretic driving force $F_m = M_{cell}$gradB. If the magnetic field gradient is uniform, once the permanent regime is reached, the determination of the cell's velocity, v_{cell}, and diameter d_{cell}, provides access to the viscous force $F_v = 3\pi\eta d_{cell} v_{cell}$ which counterbalances the magnetic one: $F_v = F_m$. The cell magnetic moment is therefore directly proportional to the cell measured velocity. Such a measurement leads to the magnetisation of individual cells, therefore being called single-cell magnetophoresis. Performed over a large number of cells, it gives access to the distribution of magnetic load over a cell population. Practically, the magnetophoresis set-up used consists of a permanent circular magnet adapted to an inverted microscope and developing, in the observation window (objective 10×, 6 mm apart from the magnet surface) a 145 mT magnetic field and a 17 mT mm^{-1} magnetic field gradient. From video analysis the velocity and the diameter of 200 cells migrating towards the magnet were measured for each incubation condition. Measurements were performed in duplicate or triplicate with different cell samples. The cells' magnetic moments measured were converted in mass of iron (expressed in pg): 6.6×10^{-14} A m^{-1} weights 1 pg of iron. This magnetophoretic measurement was previously validated with global iron quantification performed using Electron Spin Resonance (ESR).[9]

RNA isolation, cDNA synthesis and quantitative real-time RT-PCR analysis

Total RNAs from PMA-stimulated or non-stimulated cells with or without magnetic labelling were prepared using the total RNA isolation kit (Machery-Nagel), including the DNase treatment step to avoid contamination with genomic DNA. Complementary DNA (cDNA) was synthesized using SuperScript II Reverse Transcriptase (Invitrogen), from 1 μg of total RNA in a final volume of 100 μl. Real time quantitative RT-PCR was performed in duplicate with the ABI PRISM 7900 sequence Detection System and SYBRGreen dye (Applied Biosystems) according to the manufacturer's protocol. Primers were designed using Primer Express program (Applied Biosystems). mRNA levels were normalized against reference gene RPLP0 mRNA (the large P0 subunit of the acidic ribosomal phosphoprotein). Amplification of specific transcripts was confirmed by melting curve profiles generated at the end of the PCR program.

The fluorescence cycle threshold (Ct) was calculated to quantify the relative amount of gene expression. The mRNA levels of genes of interest (R) were expressed relative to levels of RPLP0, ($\Delta Ct = Ct_R - Ct_{RPLP0}$) and the relative amount of R mRNA levels between treated and non-treated cells is given by $2^{-\Delta\Delta Ct}$, where $\Delta\Delta Ct$ = [$\Delta Ct(R)$ of PMA-stimulated cells] − [mean of $\Delta Ct(R)$ of non-stimulated cells] for the same magnetic labelling.

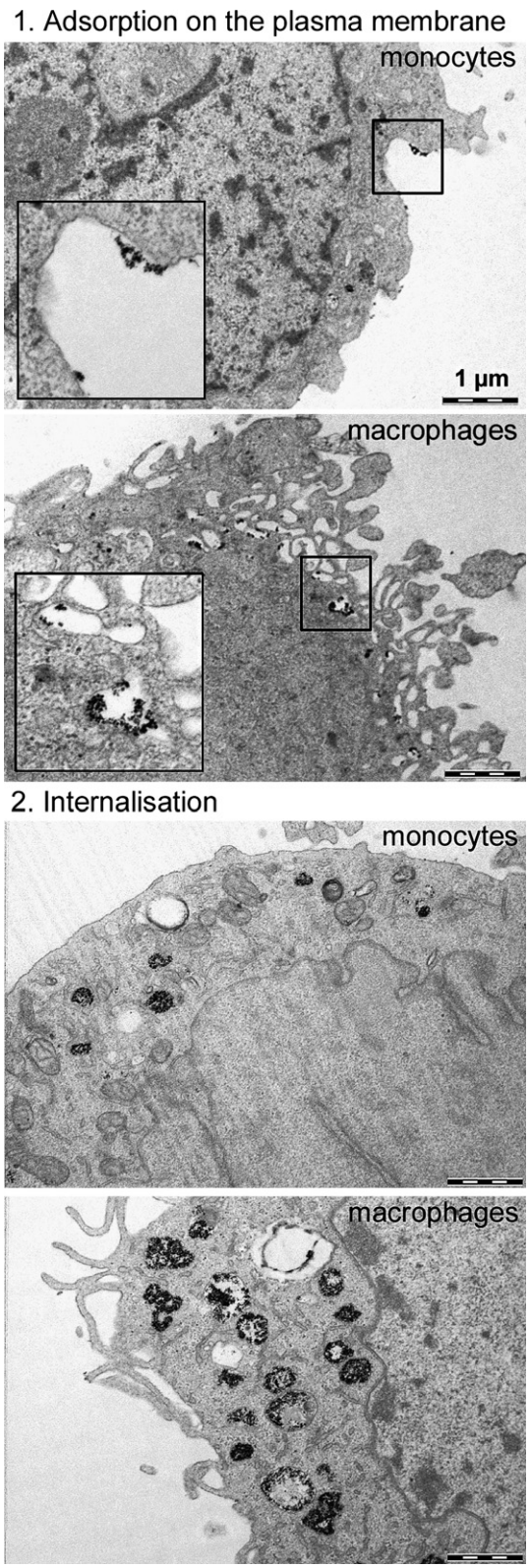

Fig. 1 Transmission electron microscopy studies were carried out to assess the localisation of nanoparticles in monocyte and macrophage cells. Incubation was performed for 2 h at 2 mM of extracellular iron, either at 4 °C (inhibiting endocytosis) or at 37 °C. At 4 °C, nanoparticles are found slightly clustered on the cell membrane. Multiple membrane folding is visible for macrophages, with more nanoparticles adsorbed on the membrane. At 37 °C, nanoparticles are internalized through the endocytic pathway and concentrate within micron-sized vesicles, resembling late endosomes and lysosomes.

Results

Cellular localisation of the nanoparticles

TEM observations were carried out to trace the interaction of the nanoparticles with the cells and their subsequent localization. Previous studies have demonstrated for cancer cell lines that the anionic magnetic nanoparticles were internalized *via* the endocytotic pathway and were sequestered in lysosomes after cell loading.[8] Our findings also suggest the endocytotic uptake of the nanoparticles by both monocyte and macrophage cells and their further localization in lysosomes. Moreover, nanoparticles endocytosis was found to be first triggered by an adsorption step on the cell outer membrane. Indeed, TEM images of cells incubated with the nanoparticles ([Fe] = 2 mM-2 h) under cold conditions (4 °C), blocking the dynamical events of endocytosis, show clustered nanoparticles on the cell membrane with no internalisation (Fig. 1.1). It is well known that the cell surface possesses many anionic large domains, consistent with the net negative charge measured by cell electrophoresis. However, it is probable that these negative domains coexist with scarcer positive ones, onto which anionic nanoparticles adsorb and that the clustering effect on the anionic nanoparticles is likely due to their repulsive interactions with the negatively charged domains.

The same incubation ([Fe] = 2 mM-2h) performed at 37 °C (and followed by one additional hour at 37 °C in nanoparticle-free medium) led to the accumulation of the nanoparticles in intracellular compartments resembling lysosomes (Fig. 1.2). Furthermore, these qualitative observations demonstrate a more important capture of nanoparticles by the macrophages compared to monocytes, both at the cell membrane and intracellularly.

Quantitative cellular iron uptake

Nanoparticle cell load was assessed by single-cell magnetophoresis. The tracking of 200 individual cells in movement at constant velocity towards a permanent magnet (magnetophoresis) allows determining the magnetic moment of each individual cell which is converted into a number of nanoparticles, or alternatively a mass of iron, expressed in pg (0.8 million nanoparticles weighting 1 pg of iron). The distribution of iron load over the cell population are represented on Fig. 2 for both monocytes and macrophages, incubated for 2 h with nanoparticles at iron concentrations 2 mM_{Fe}. The cellular uptake of nanoparticles strongly increased for macrophages compared to monocytes, both for the adsorption on the plasma membrane (4 °C incubation) or for the whole internalisation process (37 °C). The total iron uptake was found to be about 22 pg_{Fe} in macrophages compared to 3 pg_{Fe} in monocytes. Interestingly there appeared to be the same fall for the sole adsorption on the membrane (12 pg_{Fe} on macrophages membranes compared to 2 pg_{Fe} on monocytes).

In the interest of further probing the mechanism of cell internalization of these nanoparticles, quantification of the iron

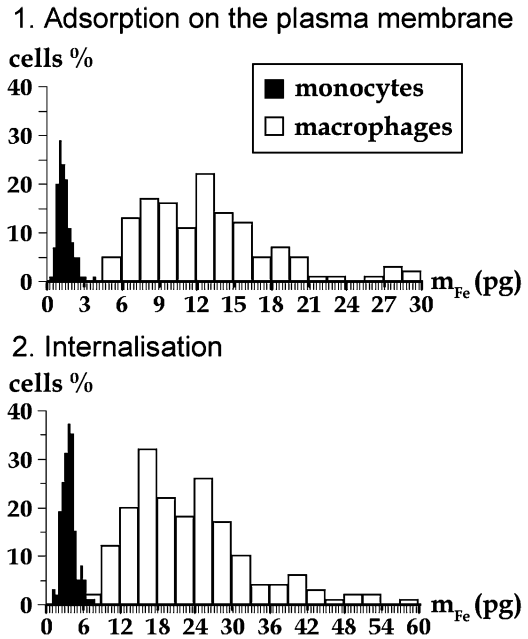

Fig. 2 Single cell magnetophoresis allows determining the iron load distribution for monocytes and macrophages. Here, cells were incubated for 2 h with 2 mM extracellular iron, at 4 °C (adsorption) or 4 °C (internalisation). Nanoparticles are taken up less efficiently by monocytes (mean iron load adsorbed of 2 pg_{Fe} $cell^{-1}$ and internalised of 3 pg_{Fe} $cell^{-1}$) than by macrophages (mean iron load adsorbed of 13 pg_{Fe} $cell^{-1}$ and internalised of 22 pg_{Fe} $cell^{-1}$). Standard deviation among the cell population is comparable for both cell types, close to 35%.

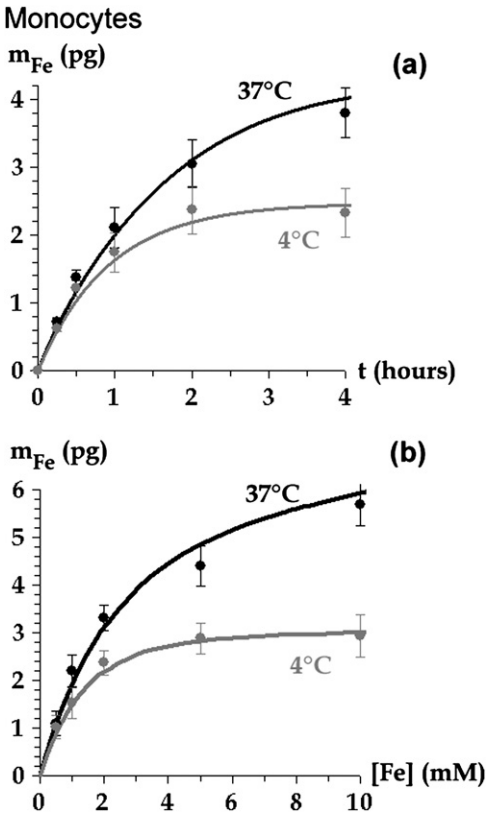

Fig. 3 Uptake curves for monocytes incubated at 4 °C and 37 °C, monitored as a function of the incubation time, t, ((a), [Fe] = 2 mM) or of the iron extracellular concentration [Fe] ((b), t = 2 h). Binding and incorporation with anionic magnetic nanoparticles were saturable with time and extracellular iron.

load was performed after incubation at different iron concentrations (from 0.5 to 10 mM_{Fe}) and incubation times (from 15 min to 4 h), both at 4 °C and 37 °C. For monocytes, saturation was found as a function of both time and extracellular iron concentration (Fig. 3). The total iron load increased up to 4 h at an extracellular concentration of 2 mM_{Fe} after which saturation at about 4 pg_{Fe} $cell^{-1}$ is observed. The same "steady-state" loading (saturation with time) was attained in approximately 2 h at 4 °C for the adsorption process and was found close to 2 pg_{Fe} $cell^{-1}$. Similarly, the loading with nanoparticles at a given incubation time (2 h) was saturable with extracellular iron concentration, attaining a maximum at about 6 pg_{Fe} $cell^{-1}$ for the total uptake at 37 °C and 3 pg_{Fe} $cell^{-1}$ for the sole membrane adsorption.

By contrast, if the nanoparticles adsorption on the macrophages membranes again saturates with both time (maximum of 12 pg_{Fe} $cell^{-1}$ reached in 2 h at 2 mM_{Fe} extracellular concentration) and iron concentration (maximum of 18 pg_{Fe} $cell^{-1}$ for a given 2 h incubation time attained at 5 mM_{Fe} extracellular concentration), no saturation is yet observed at 4 h (almost 40 pg_{Fe} $cell^{-1}$ internalised) for 2 mM_{Fe} and saturation is initiated at 10 mM_{Fe} (44 pg_{Fe} $cell^{-1}$) but not yet attained for a 2 h incubation time (Fig. 4).

Modelling the cell capture

We demonstrated both qualitatively and quantitatively that the nanoparticles show a strong affinity for the cell membrane, leading to their spontaneous adsorption, which in turn triggers the internalisation *via* the endocytotic pathway. The overall uptake was described as a two-step process which occurs concomitantly: (1) Binding of nanoparticles on reactive sites on the cell membrane, (2) Internalisation of the reactive sites by endocytosis pathway. Our asset is that we provided the kinetics of nanoparticle capture at 4 °C, excluding any internalisation to occur. We could then model as a first step the binding process itself. A Langmuir mechanism with adsorption and desorption constants k_a and k_d (expressed respectively in M_{Fe}^{-1} s^{-1} and in s^{-1}) defines the adsorption step as follows:

$$\frac{dm}{dt} = k_a[\mathrm{Fe}](m_o - m) - k_d m \quad (1)$$

This equation simply means that the adsorption rate of nanoparticles on the cell surface is proportional to both the extracellular iron and the number of vacant binding sites ($m - m_o$) (m_o being the binding capacity, that is the maximum mass of iron that can be adsorbed) while the desorption rate is proportional to mass, m, already adsorbed. Experimental measurements presented in Fig. 3 and 4 (grey symbols) are well adjusted by eqn (1) (plain grey lines). The parameters k_a, k_d and m_o obtained are given in Table 1 for both macrophages and monocytes. These parameters could then be used as a second step to model the overall uptake, including the concomitant mechanisms of adsorption and internalisation. The only internalisation

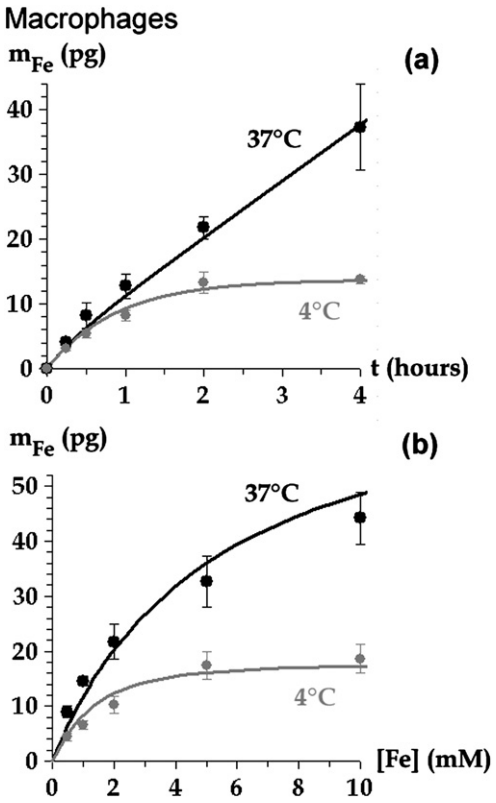

Fig. 4 Uptake curves for macrophages incubated at 4 °C and 37 °C, monitored as a function of the incubation time t ((a), [Fe] = 2 mM) or of the iron extracellular concentration [Fe] ((b), t = 2 h). In the range of experimental conditions (1–4 h, 1–10 mM_{Fe}), binding was saturable with time and extracellular iron, while internalisation does not reach saturation with time and starts only saturating with extracellular iron.

process was then seen as the internalisation by endocytosis pathway of the reactive membrane sites associated with a mass m_{ext} of nanoparticles:

$$\frac{dm_{int}(t)}{dt} = \frac{d\Phi_{int}(t)}{dt} m_{ext}(t) \quad (2)$$

$\Phi_{int}(t)$ being the fraction of the reactive surface being internalized at time, t, over the total reactive surface. We hypothesized a first-order kinetic law to describe this endocytotic process:

$$\frac{d\Phi_{int}(t)}{dt} = k_i(\Phi_o - \Phi_{int}(t)) \quad (3)$$

with Φ_o the maximum fraction of the reactive surface that can be internalized by the cell and k_i the rate constant for internalization (expressed in s^{-1}).

To adjust the experimental data presented in Fig. 3 and 4 for the overall nanoparticles capture (black symbols), we solved numerically eqn (2) and (3) together with the following eqn (4) governing the time dependence of m_{ext}, taking into account both the binding process and the internalized mass:

$$\frac{dm_{ext}(t,[Fe])}{dt} = k_a[Fe](m_o - m_{ext}(t)) - k_d m - \frac{dm_{int}(t)}{dt} \quad (4)$$

Note that the total mass, m, measured is simply $m = m_{int} + m_{ext}$. The only adjustable parameters are then Φ_o and k_i, which are given in Table 1 for both macrophages and monocytes, as obtained from the fits (presented as plain black lines in Fig. 3 and 4).

Differentiation of monocytes into macrophages after magnetic labelling

One concern arising from magnetic labeling of monocytes is their capability to differentiate into macrophages when loaded with nanoparticles and the subsequent fate of the nanoparticles after cell differentiation. This question is particularly important for applications where circulating monocytes are labelled *in vivo* (after iv administration of nanoparticles) or directly injected after *in vitro* labelling. As a first step, we verified by trypan blue and proliferation assays that cell labelling did not impair monocyte viability (data not shown). As a second step, we investigated whether labelled monocytes could differentiate into functional macrophages. To do so, we carried out two functional assays: (1) morphological characterisation of macrophages differentiated from magnetically labelled monocytes and (2) genetic checking of the expression of two macrophage representative genes: CD68, a specific marker expressed by human tissue macrophages[10] and the membrane receptor EMR1, a myeloid-related gene of the mononuclear phagocyte system.[11]

Monocyte labelling was achieved after incubation with nanoparticles at extracellular iron concentrations from 0.5 to 5 mM and incubation time 2 h, resulting in a maximal iron oxide uptake of 4 pg_{Fe} $cell^{-1}$. For all incubation conditions, after six-day stimulation with phorbol esters (PMA), monocytic cells adhered and show similar morphology as control cells, as observed by transmission microscopy (40− objective, Fig. 5a) and electron microscopy (Fig. 5b). Number of adherent cells after 6-days stimulation was equal whether they derived from labelled or non-labelled monocytes. Monocyte death after 8-days of differentiation treatment was found about 76% whatever the labeling conditions ((75.4 ± 1.8)% for control cells and (76.5 ± 2.6)%, (77.7 ± 2.5)% for monocytes labeled with 2 and 5 mM_{Fe}, respectively). Lysosomal vesicles filled with nanoparticles are seen in the perinuclear region. Nanoparticles appear more

Table 1 Parameters describing the cellular uptake for monocytes and macrophages.[a]

	d/μm	$k_a/M_{Fe}^{-1}\ s^{-1}$	k_d/s^{-1}	m_o/pg	Φo	k_i/s^{-1}
Monocytes	13.4 ± 1.5	0.117 ± 0.005	$6.6 \pm 1.8 \times 10^{-5}$	3.2 ± 0.2	1.4 ± 0.2	$3.9 \pm 0.5 \times 10^{-4}$
Macrophages	20.4 ± 3.7	0.119 ± 0.007	$7.5 \pm 1.3 \times 10^{-5}$	18.4 ± 1.8	19 ± 1	$2.2 \pm 0.7 \times 10^{-4}$

[a] d: cell diameter. k_a: adsorption constant. k_d: desorption constant. m_o: maximal iron mass that can adsorb on the membrane. k_i: time constant. Φ_o: fraction of internalised active surface (on which nanoparticles are first adsorbed).

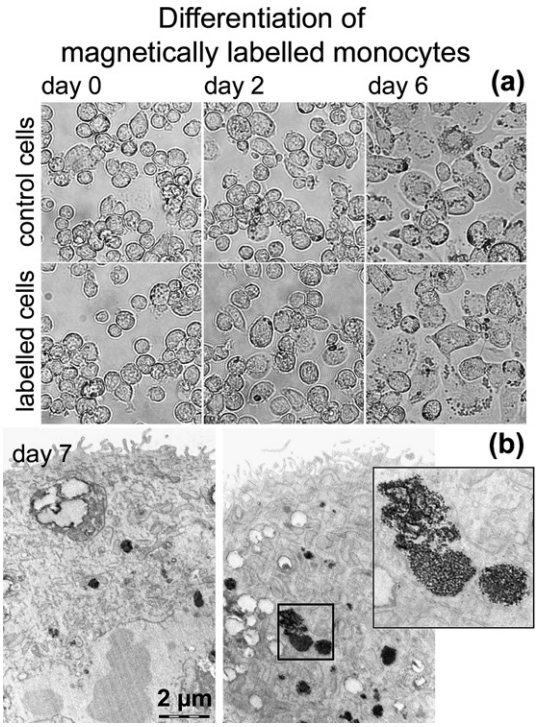

Fig. 5 Optical (a) and electron (b) microscopy images of monocytes first labelled with anionic magnetic nanoparticles for 2 h at 2 mM of extracellular iron (3 pg_{Fe} $cell^{-1}$) and then further differentiated into macrophages by 6-days PMA stimulation. Cell morphology resembles control non-labelled macrophages (a, 40× magnification). Nanoparticles appear highly concentrated within lysosomes that are found more or less abundant within the cytoplasm (b).

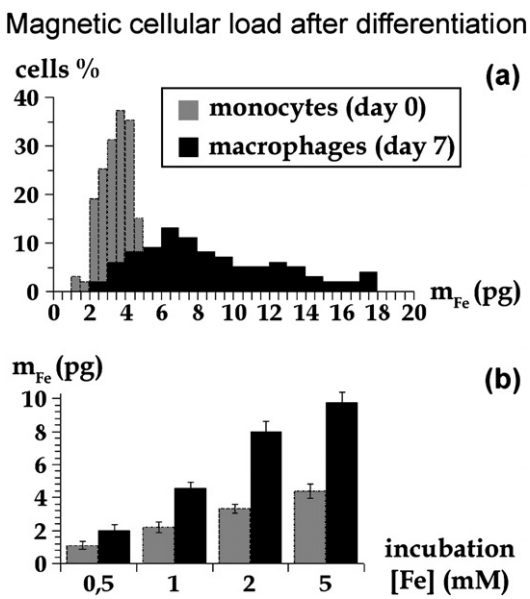

Fig. 6 Quantification of the iron load after the 6-day differentiation process. Monocytes were incubated for 2 h at 0.5, 1, 2 and 5 mM_{Fe} with corresponding iron load from 1.5 to 4 pg_{Fe} $cell^{-1}$. For the 2 mM_{Fe} condition, distribution of the iron load is shown in (a). After the differentiation, the iron load is higher, in the range 2 to 10 pg_{Fe} $cell^{-1}$ for the four conditions (b), and much more distributed (a) with standard deviation in between 50 and 60%.

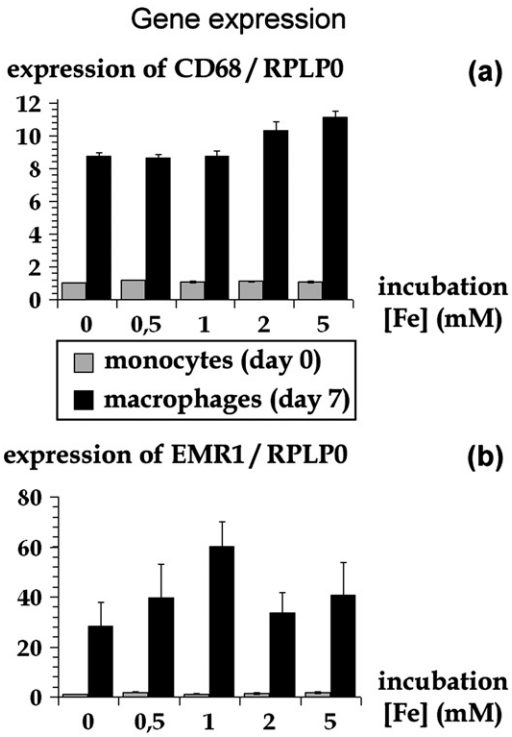

Fig. 7 CD68 (a) and EMR1 expression (b) in THP-1 cells with or without PMA treatment. Levels of CD68 and EMR1 mRNA were measured by real-time PCR, normalized to RPLP0 mRNA. THP-1 cells unlabelled or labelled with 0.5, 1, 2 or 5 mM of maghemite nanoparticles, then stimulated or not with 50 ng ml^{-1} PMA were used to prepare total RNA according to the experimental procedure. Increases in CD68 and EMR1 gene expression in cells stimulated with PMA were compared with corresponding non-stimulated cells. Results are expressed in arbitrary units (mean ± SEM) using the "$2^{-\Delta\Delta Ct}$" formula with the control values taken as 1.

packed within the vesicles after 6-days of differentiation treatment (inset in Fig. 5).

Moreover, nanoparticles appear much more distributed among the macrophage cell population, with cells containing a large number of magnetic lysosomes and others with much more sparse magnetic lysosomes. This TEM observation was further confirmed by magnetophoretic iron quantification for the macrophages derived from magnetically-labelled monocytes. Mean iron content in macrophages was about twice the one in the precursor labelled monocytes (Fig. 6) and the standard deviation over the cell population increased from 35% for the monocytes to 50 to 60% for the macrophages issued from the labelled monocytes after 6 days PMA stimulation. By comparison, direct labelling of macrophages (Fig. 2) led to a standard deviation of 35%. This increase of mean iron load $cell^{-1}$ and of dispersion within the cell population could be related to constitutive cell death during the differentiation process and phagocytosis of cell debris, including the nanoparticle cargo.

Finally, the expressions of CD68 and EMR1 genes were investigated in order to check possible alteration of phagocytosis capability as a result of nanoparticle uptake. Total RNA from cells was extracted directly after magnetic labelling (day 0) or

after 6-days PMA treatment (day 7). The level of CD68 and EMR1 mRNA expression was measured by quantitative real-time PCR. Magnetic labelling does not alter CD68 and EMR1 mRNA expression for precursor monocytes, leading to the initial level of each gene expression. The 6-day PMA stimulation of control non-labelled monocytes increased the CD68 expression by 8.8 ± 0.2-fold (Fig. 7a) and the EMR1 expression by 28.2 ± 9.5-fold (Fig. 7b). For monocytes labelled with different extracellular concentration (0.5, 1, 2 and 5 mM_{Fe}), the same increase was observed, demonstrating that the magnetic label did not affect the expression of genes reflecting macrophage phagocytosis capacity.

Discussion

Monocytes and macrophages play key roles in numerous inflammatory diseases including atherosclerosis, multiple sclerosis, ischemic stroke lesions, sepsis, local brain inflammation, transplanted graft rejections, and many others. There is therefore a large clinical need for a non-invasive tool to assess monocytes and macrophages infiltration *in vivo*, during inflammatory events. MRI cell imaging using iron oxide nanoparticles as a cellular contrast agent have been developed during the last decade as a method of choice to track cell migration in living animals.[1,2] The prerequisite for the establishment of an efficient MR imaging method to follow the fate of monocytes and macrophages is the capture of MRI contrast agents as magnetic nanoparticles by the cells. The key issues that require to be tackled prior to the imaging applications are (1) the mechanism of interactions of nanoparticles with the monocyte/macrophage system and (2) the biological effect of iron oxide uptake on the cell functions, in particular the capacity of labelled monocytes to differentiate into macrophages.

Macrophages magnetic labelling has been widely investigated this last decade using dextran-coated iron oxide nanoparticles. Nanoparticles are then internalised within macrophage cells by fluid-phase endocytosis. Numerous labelling procedures were conducted, the inferred magnetic load varying from one order of magnitude. Typical values are presented for instance for peritoneal mouse macrophages (10 pg_{Fe} $cell^{-1}$)[12] or rat macrophages (4 pg_{Fe} $cell^{-1}$),[13] or for freshly isolated human macrophages (15 pg_{Fe} $cell^{-1}$).[14] Here we characterized the uptake mechanism of anionic iron oxide nanoparticles within THP1 monocytes cultured *in vitro* and in the derived macrophages which resemble in many criteria native monocyte-derived macrophages. We demonstrated that, as previously observed for other cell types as cancer cells or therapeutic cells,[8] the nanoparticles were taken up by an "adsorptive endocytosis" pathway.[8] The overall uptake was then modeled as a two-step process including a non-specific interaction with the cell plasma membrane which precedes the internalisation. Interestingly, the affinity $K = k_a/k_d$ of the nanoparticles for the cell membrane was found identical for monocytes and macrophages, of the order of 2.0×10^3 M_{Fe}^{-1}, or equivalently 2.0×10^7 $M_{nanoparticles}^{-1}$. This affinity corresponds to the one obtained for other cell types as cancer cells. By contrast, the maximum mass of iron m_o that can adsorb on the membrane was more important for macrophages (18 pg_{Fe} $cell^{-1}$) than for monocytes (3 pg_{Fe} $cell^{-1}$). This first reflects differences in cell diameter for the two cell types (13.7 μm for monocytes *versus* 20.4 μm for macrophages). However, the maximal mass per unit surface for monocytes was close to the one obtained for HeLa tumour cells, whereas it was from two to three times higher for macrophages. This enhanced membrane adsorption is probably due to multiple macrophage membrane folding as observed on electron microscopy images (Fig. 1). Overall uptake of anionic nanoparticles results from concomitant adsorption and internalisation process, leading to an excellent efficiency of the magnetic labelling: we report a maximum load of 6 pg_{Fe} $cell^{-1}$ in monocytes and almost 50 pg_{Fe} $cell^{-1}$ in derived macrophages. Interestingly, the internalisation process clearly depends on the differentiation state of the cells: reflecting their important phagocytic activity, macrophages were able to internalise nearly 2000% of the membrane accessible to the nanoparticles, compared to only 140% for the monocytes.

We next demonstrated that the monocytes magnetic labelling does not impair their ability to differentiate into macrophages. This is in agreement with the recent study investigating the effect of the incorporation of iron oxide agents coupled with protamine sulfate within THP1 cells and demonstrating no impairment of the immunological properties of macrophages due to the magnetic label.[15]

The substantial contributions of the present study are two-fold. First we fully characterized the overall uptake mechanism of the incorporation of anionic magnetic nanoparticle agents into both monocytes and macrophages, allowing comparing adsorptive and internalisation capacities. Adsorption on the macrophages plasma membrane is enhanced probably due to the presence of multiple membrane folding. More importantly, the internalisation capacity of macrophages is more than ten times the one of monocytes. These observations could be of importance when evaluating this class of anionic contrast agents for applications involving their capture by macrophages *versus* monocytes *in vivo* after intravenous injection (for instance to identify inflammatory and degenerative disorders involving strong phagocytic activity of macrophages). However, one must keep in mind that opsonization may significantly change the nanoparticle properties. Second, we obtained an iron uptake in non-stimulated monocytes of up to 6 pg_{Fe} $cell^{-1}$, without impairment of their capacity to differentiate into macrophages and with a significantly increased iron load in derived macrophages. This labelling is large enough to permit MRI detection, with following cellular imaging applications as tracking of labelled monocytes, recruitment at inflammation, up to differentiation into macrophages. Of course the monitoring of magnetically labelled macrophages is as well promising for clinical applications.

Conclusion

To conclude, here we established that anionic magnetic nanoparticles are very efficiently captured by the monocyte–macrophage system, with an enhanced uptake in macrophages regarding both the adsorptive step on the plasma membrane and the internalisation capacity. Moreover, the incorporation of the nanoparticles did not alter differentiation of monocytes into macrophages.

References

1 M. Modo, M. Hoehn and J. W. Bulte, *Mol. Imaging.*, 2005, **4**, 143–64.
2 W. J. Rogers, C. H. Meyer and C. M. Kramer, *Nature Clin. Pract. Card. Med.*, 2006, **3**, 554–562.
3 C. Corot, K. G. Petry and R. Trivedi *et al.*, *Invest. Radiol.*, 2004, **39**, 619–625.
4 V. Amirbekian, M. J. Lipinski and K. C. Briley-Saebo *et al.*, *Prod. Nat. Acad. Sci.*, 2007, **104**, 961–966.
5 P. Smirnov, M. Poirier-Quinot and C. Wilhelm *et al.*, *Magn. Res. Med.*, 2008, **60**, 1292–1297.
6 M. R. Choi, K. J. Stanton-Maxey and J. K. Stanley *et al.*, *Nano Lett.*, 2007, **7**, 3759–65.
7 A. Beduneau, Z. Ma and C. B. Grotepas *et al.*, *PLoS ONE*, 2009, **4**, e4343.
8 C. Wilhelm and F. Gazeau, *Biomaterials*, 2008, **29**, 3161–3174.
9 C. Wilhelm, F. Gazeau and J. Roger *et al.*, *Langmuir*, 2002, **18**, 8148–8155.
10 K. A. Pulford, A. Sipos, J. L. Cordell, W. P. Stross and D. Y. Mason, *Int. Immunol.*, 1990, **2**, 973–980.
11 D. A. Hume, *Curr. Opin. Immunol.*, 2006, **18**, 49–53.
12 A. Moore, E. M. Marecos, A. Bogdanov and R. Weissleder, *Radiology*, 2000, **214**, 568–74.
13 I. Siglienti, M. Bendszus, C. Kleinschnitz and G. Stoll, *J. Neuroimmun.*, 2006, **173**, 166–173.
14 K. Müller, J. N. Skepper and M. Posfai *et al.*, *Biomaterials*, 2007, **28**, 1629–1642.
15 B. Janic, A. S. Iskander, A. M. Rad, H. Soltanian-Zadeh and A. S. Arbab, *PLoS ONE*, 2008, **3**, e2499.